Shade Happens: GHG emissions-driven analysis of BIPV strings under partial shading

Citation for the original published paper (version of record):
McCarty, J., Galimshina, A., Waibel, C. et al (2025). Shade Happens: GHG emissions-driven analysis of BIPV strings under partial shading. IOP Conference Series: Earth and Environmental Science, 1554(1). http://dx.doi.org/10.1088/1755-1315/1554/1/012045

IOP Conference Series:
Earth and
Environmental Science

PAPER • OPEN ACCESS

Shade Happens: GHG emissions-driven analysis of BIPV strings under partial shading

To cite this article: J McCarty *et al* 2025 *IOP Conf. Ser.: Earth Environ. Sci.* **1554** 012045

IOP Conf. Series: Earth and Environmental Science **1554** (2025) 012045 doi:10.1088/1755-1315/1554/1/012045

Shade Happens: GHG emissions-driven analysis of BIPV strings under partial shading

J McCarty[1,5], A Galimshina[2,5], C Waibel[1,3,5], A Hollberg[4,5], and A Schlueter[1,5]

[1]Chair of Architecture and Building Systems, ETH Zurich, Zurich, Switzerland
[2]Civil Engineering, Architecture and Arts Institute, Nosov Magnitogorsk State Technical University, Russia
[3]Flemish Institute for Technological Research (VITO), Mol, Belgium
[4]Department of Architecture and Civil Engineering, Chalmers University of Technology, Gothenburg, Sweden
[5]Future Cities Laboratory, ETH Zurich, Zurich, Switzerland

E-mail: jmccarty@ethz.ch

Abstract. The interconnection of photovoltaic (PV) modules into series and parallel connections has garnered significant attention in the literature over the past decade. The connection is typically fixed for the system's service life and can heavily dictate the system's performance if it encounters partial shading. In building-based applications of PV, this issue has not received as much attention due to the prevalence of module-level power optimisers and microinverters as a solution to partial shading. However, these types of devices have the potential to negatively impact the carbon-emissions abatement potential of systems if not used with a critical lens to their life-cycle environmental impact. In this paper, we compare the system performance of seven different PV interconnection schemes using carbon payback time. We model a building-integrated photovoltaic (BIPV) facade and simulate its annual yield at an hourly timestep. We use a current and voltage curve approach to capture the impact of partial shading. We find that module-level optimiser-based systems are capable of generating enough electricity to offset the carbon emitted during their manufacturing in the context of Zurich, Switzerland. Furthermore, we discuss future research directions for BIPV string optimisation.

1 Introduction

Photovoltaics (PVs), particularly building integrated photovoltaics (BIPVs), are becoming a more common fixture in urban settings, often with the goal of mitigating greenhouse gas (GHG) emissions. However, if a PV system is deployed in a situation where it is unable to abate or mitigate an adequate amount of carbon emissions to offset the upfront GHG emissions released during its manufacturing, it may act as a source of further pollution. The performance level of a system, in terms of GHGs, can be tied to many features, but is most simply visualized as a function of the amount of irradiance available to the system throughout the year. We describe this through the curve in Figure 1, which shows the range GHG intensities (E_{int}) [$\frac{\text{kgCO}_2\text{e}}{\text{kWh}}$] of a theoretical PV system in Zurich, Switzerland given different levels of effective irradiance (G_{eff}) [$\text{kWh} \cdot \text{m}^{-2} \cdot \text{year}^{-1}$]; with low G_{eff}, E_{int} is high and the opposite with high levels of G_{eff} in a non-linear relationship. From previous research [1] we can overlay the range of G_{eff}

levels of G_{eff} in a non-linear relationship. From previous research [1] we can overlay the range of G_{eff} found on the exposed surfaces of buildings in a quarter of Zurich (the grey histogram). By also indicating the typical E_{int} of Switzerland's electricity grid (the horizontal black line), we can showcase that there are surfaces where installing a system would likely result in it not performing as well as the local electricity grid in terms of E_{int}.

This issue can also be seen in practice. Using a post-installation report of a BIPV facade system in Zürich, Switzerland [3] that describes annual electricity generation we can calculate the expected payback period for the upfront carbon of the modules, following [4]. This carbon payback time (CPT) ranges from 12 years for the rooftop array to 128 years for the north-facing array, with a 45-year payback for the entire system when aggregated; the expected operational lifetime of the system is 25 years. Following these calculations, it can be seen that this system (as a whole) is not contributing to GHG mitigation. Given this realisation, it is clear that carbon payback should be a key performance indicator for system design. Furthermore, due to a lack of reported hourly electricity generation data, a static value for E_{int} of the grid was assumed. When considering a dynamic grid emissions factors, which we do in the methodology of this paper, CPT might be even higher.

1.1 Objectives

Losses within a PV system, which contribute to less GHG mitigation, can be attributed to several factors: soiling, temperature, device deficiencies, cell degradation, and electrical mismatch. In this study, we focus on the engineering of PV systems to reduce losses related to electrical mismatch and the embodied carbon related to those engineering choices. PV systems are typically comprised of interconnected modules, either in series or parallel, to engineer a system's current (I) and voltage (V) output to desired levels and to mitigate losses associated with electrical mismatch. In PV deployment cases where surface irradiance is not homogeneous (i.e. partial shading), the modules will output different I and V, making it problematic to tie them together, as a function within the system known as the maximum power point tracker (MPPT) will restrict the power of the interconnected string to the lowest performing module—likely the module with the least G_{eff}. As these conditions are more common in urban BIPV settings, module interconnections are typically minimised to ensure MPPT is being done on either two modules or in many cases, a single module. In this paper, we model a BIPV facade and compare various interconnections to module-level MPPT using the time to payback (i.e. offset) the system's upfront carbon (i.e. CPT). Using CPT ensures that we not only account for differences in the embodied carbon of the various interconnection designs, but also account for the dynamics of emissions abatement from the electricity generated. Our hypothesis assumes that the module-level MPPT systems may generate the most electricity, but will not have the fastest CPT due to their higher embodied carbon. The importance of this may not be apparent, but as shading is a temporally-dynamic feature, it is expected that the capacity of different interconnections to mitigate its influence will not be the same during each of hour of the day. For example, during the afternoon hours of an Autumn day, Interconnection System 1 (IS1) may perform better than Interconnection System 2 (IS2). However, due to some particularities of IS2, it may perform better during Autumn mornings when the emissions factors associated with the electricity

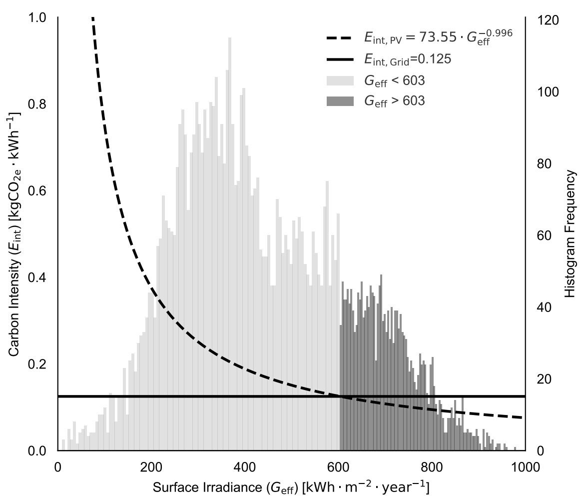

Figure 1: The curved dashed line indicates the lifetime emissions intensity of generated electricity from a monocrystalline system (efficiency=20.7%, embodied=329-$\text{gCO}_{2\text{e}}\text{m}^{-2}$) under various levels of surface irradiance, assuming no annual losses except for those related to temperature and that all generated electricity offsets CO_2 from the electricity grid. Using the horizontal line, this curve is compared to the Swiss grid emissions factor of 0.125-$\text{kgCO}_{2\text{e}} \cdot \text{kWh}^{-1}$ per [2]. The histogram represents the range of solar potentials (G_{eff}) in a district of Zurich [1]. The shift in the histogram's lightness represents surfaces that fall below the point at which the emissions intensity of the PV system and the electricity grid intersect (603 $\text{kWh} \cdot \text{m}^{-2} \cdot \text{year}^{-1}$).

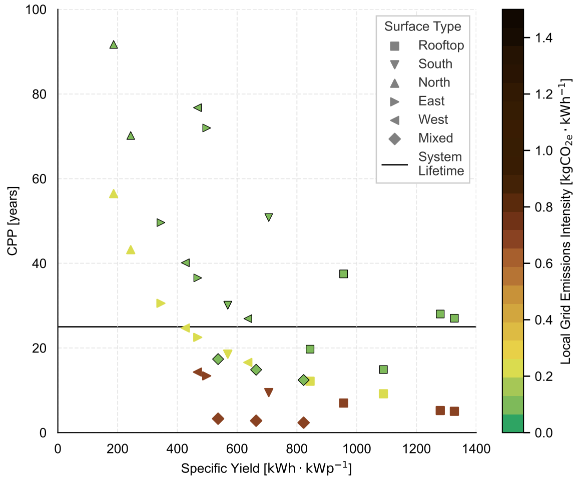

Figure 2: Examples of assessed CPT and specific yield for several PV projects found in the literature. Markers with a black edge are recalculated from the literature data using a E_{int} of 0.125-kgCO$_{2e}$ · kWh^{-1} for Switzerland from the KBOB [2]. The mixed category is of results from whole building studies where both monocrystalline and polycrystalline modules were installed on facades and rooftops—the results were only reported as an aggregate.

grid are much higher than in the afternoon. To capture this, we also utilise hourly emissions values for the grid electricity that is being offset by the PV system-generated electricity.

1.2 Background

Interconnections There has been research on PV module interconnection using conventional and hybrid approaches [5, 6, 7, 8], as well as optimisation work done on PV interconnection in complex BIPV facades [9, 10]. While there has been BIPV facade design work around module placement sensitivity [11], the accounting for the embodied carbon of interconnection devices in the carbon payback time of the system is a contribution to the field. Furthermore, there has not been an extensive comparison of interconnection design for BIPV facades in a real array. Typically, theoretical and simple arrays are analysed (i.e. a standard grid of the same-sized modules). The often complex nature of BIPV facade arrangements necessitates the use of less-conventional string layouts to maximise power output and minimise embodied carbon as typical stringing cannot be applied effectively. This approach will provide the system with the best chance of being a net-benefit carbon emissions mitigation/abatement tool.

Carbon Payback In Figure 2 the specific yield [kWh · kWp^{-1}] and CPT of several case studies in the literature can be seen [12, 13, 14]. For these examples, we additionally plot—in the markers with black edges—a recalculation of CPT using the E_{int} for Switzerland from Figure 1 of 0.125 to show its influence on the overall performance of a system relative to a 25-year lifetime. We find that in the majority of the original cases, the payback time is less than 25 years. However, for most of these cases, once the grid intensity is shifted to the lower value, the system is no longer able to mitigate more carbon than was required to manufacture and install the system. We note several exceptions, namely the mixed category in Amoruso et al. (2023) [14]. These are simulated case studies of whole-building BIPV systems including multiple technologies installed on facades and rooftops.

2 Methods

In this section, we describe the various aspects of the methodology. Initially, a well-documented BIPV facade [3] was modelled (Section 2.1) and hourly annual irradiance was simulated for a sensor grid on the facade (Section 2.2). Then, the IV-curves (i.e. the current and voltage curves) of the individual PV modules in the facade were characterised (Section 2.3). This allowed for the comparison of different interconnection schemes of the PV modules (Section 2.4) for the entire facade. The generation and loss of each of the examined interconnections was then analysed to understand which was the most performative with respect to the carbon emissions approach of this study (Section 2.5).

2.1 Modeling

A single BIPV facade oriented 65° west of South with an 183-sqm. monocrystalline array and urban context was modelled based on a prominent BIPV project in Zurich, Switzerland, located near 47°23'36.6"N 8°32'17.2"E, using approximations of the modules, images of the facade, and open data from Stadt Zurich [15, 16] as reference. An elevation view of the model can be seen in Figure 3. The array is comprised of multiple module sizes based on a 54-cell module with 3-bypass diodes and 275-Wp capacity—LG275N9K

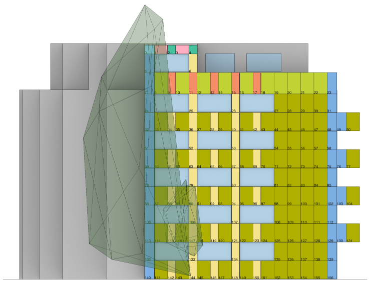

Figure 3: An elevation of the building/site model and the BIPV facade used this analysis. The coloring of the facade indicates modules of the same capacity. The facade is oriented to face 65° west of South and consists of 183-sqm. of BIPV modules.

Table 1: The seven interconnection logics followed for this study.

Interconnection	**Description**	**Module Connection**
Module-Level Conversion (MLC)	Each module has its own power optimizer performing MPPT and delivering power to a common DC backbone.	One optimizer per module
Dual-Module Conversion (DMC)	Pairs of adjacent modules are connected to an optimizer.	Two modules in series per optimizer
Series-Parallel Rows (SPR)	Modules of the same size in the same row are connected in series; rows form strings connected in parallel to a single optimizer.	Same-row modules in series → strings in parallel
Series-Parallel Floor (SPF)	Modules of the same size in two adjacent rows (representing one building floor) are connected in series; strings are then connected in parallel to an optimizer.	Modules from two adjacent rows in series → strings in parallel
Series-Parallel Columns (SPC)	Modules of the same size in the same column are connected in series; strings are then connected in parallel.	Same-column modules in series → strings in parallel
Total Cross Tied - Row (TCT-R)	Series strings formed by rows; intermediate cross-ties between strings to allow current sharing; all strings then connected in parallel.	Series per row → cross-tied → parallel
Total Cross Tied - Column (TCT-C)	Series strings formed by columns; intermediate cross-ties between strings; all strings then connected in parallel.	Series per column → cross-tied → parallel

in System Advisor Model was selected due to its similar dimensions as the modules in the actual array. The actual array is comprised of modules with a grey tint, which was not modelled due to the focus of the study being on interconnection schemes and not output. However, we note that this would lead to the overall reduction of generation in the system as the colour treatment would reflect more inbound solar radiation.

2.2 Irradiance simulation
Radiance-based ray tracing [17] on a 10-cm × 10-cm sensor grid was implemented for the facade to generate an irradiance map that was later used in the IV-curve characterization. The Radiance recipe is the enhanced 2-Phase DDS method presented in Subramaniam (2017) [18] using the following parameters: rflux [-lw 0.0001 -ab 5 -ad 10000]; rcontrib [-ad 256 -lw 1.0e-3 -dc 1 -dt 0 -dj 0]. The boundary conditions for the simulation were extracted from a weather file for Zurich [19]. Using this method the annual hourly direct and diffuse irradiance was characterized for each sensor point on the facade.

2.3 IV-curve characterization
For each hour of the year and each PV cell in each module in the facade array, an IV-curve was characterised from the cell/module parameters of the modelled module and the direct and diffuse components

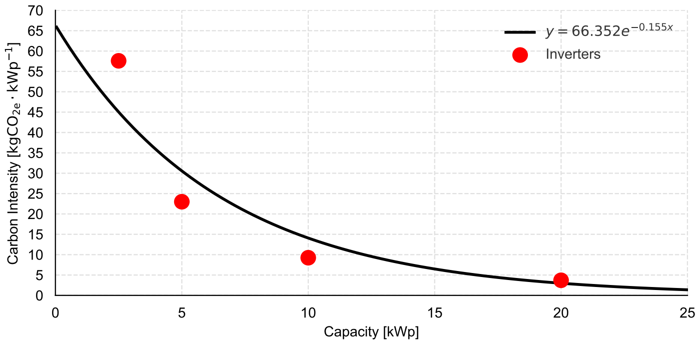

Figure 4: The power capacity and embodied carbon values from the four inverters in the KBOB database [2] were used to create a regression to facilitate the embodied carbon assessment of the various interconnections.

of irradiance. At the cell level these irradiance components were collected using a nearest point approach (i.e. the irradiance sensor point nearest to the cell center point) and converted to G_{eff} at the cell-level to account for the properties of the front cover (i.e. 4mm solar glass) of the PV module following [20]. Then single diode approach with reverse bias characterisation of [21] was used to generate the initial IV-curves, employing the framework in McCarty et al. (2024) [20]. As each cell in each module was initially characterised before combining them into the total IV-curve for the module, a module interconnection map was used to describe the module series stringing and the placement of the bypass diodes. This bypass map was only applied for the primary module (i.e. 54-cell). The other modules in the array were modelled with modified versions of bypass diode mapping, generally with rows and columns removed from the original map to match the modelled module configuration. All modules were modeled with at least 2 bypass diodes. This approach resulted in a library of IV-curves for each module in the array that could be connected using the different interconnections explored.

2.4 Module interconnections

The interconnection of PV modules in a direct current (DC) array is done to accomplish three primary tasks: (1) determining optimal current and voltage operation of the array for the electrical backbone that the power generated will be utilized from, (2) mitigating the losses due to electrical mismatch amongst the interconnected modules, and (3) reduce overall cost relative to using a module-level optimizer and MPPT. We tested seven different logics for interconnecting the modules (i.e. interconnection schemes) within an array, which are described in Table 1. As the comparison between schemes was of interest and not the impact of inverting DC to alternating current (AC), only DC-DC systems were assumed. Therefore, DC-DC optimisers were modelled at various levels within the facade for the interconnections and power generation was extracted for each hour of the year. As interconnections were constructed in the simulation, the capacity of each string in the array was totalled and used to size an optimiser. Additionally, to extract power from the final curves, the maximum power from the combination of the I- and V-curves was taken.

2.5 Carbon emissions accounting and analysis

The selected optimiser capacity of each interconnection scheme was used to calculate the global warming potential (GWP) associated with the optimiser(s) of the array using an exponential decay function that was fit to four PV inverters found in the Swiss database for construction products and processes (i.e.

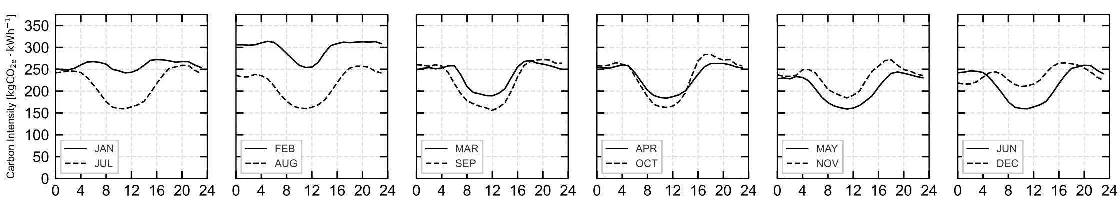

Figure 5: Typical (median) daily emissions profiles for each month that were extracted from the annual hourly emissions data used in this study.

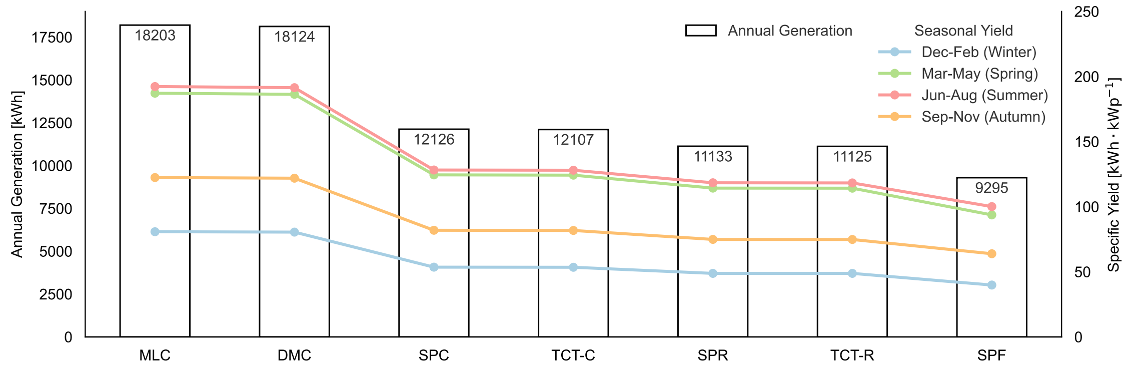

Figure 6: The annual generation of each of the interconnections is shown on the right axis in the bar plot and the seasonal specific yield is shown on the right in the line plot.

Koordinationskonferenz der Bau- und Liegenschaftsorgane der öffentlichen Bauherren), often referred to as KBOB [2]—KBOB uses a whole life cycle accounting (i.e. manufacturing through take back and recycling) for the inverter data. The four inverter values were used to fit the function, shown in Figure 4, solving GWP for the total capacity of the of PV panels configured in an interconnection.

For each of the interconnections, we simulate annual hourly electricity generation and assume that every kWh of electricity generated by the array abates the need to consume a kWh of grid-based electricity. Furthermore, we assume that this abatement of electricity consumption ends in a would-be used kWh of electricity from the grid never being generated. Therefore, there would be carbon emissions, leading the PV-generated electricity to mitigate the emissions of the electricity grid. To account for this on an hourly resolution, we use an hourly electricity grid emissions profile that is a composite of the European Union nations and Switzerland for the year 2023. This was compiled using a population weighted-average method with country profiles for population from Eurostat [22] and annual hourly emissions for each nation from ElectricityMaps (2025) [23] and has an annual mean of 237-$gCO_{2e} \cdot kWh^{-1}$, with the seasonality that can be seen in Figure 5. To account for the potential lifetime abatement, the electricity generation was projected for each year over the lifetime of the PV array, which was assumed at 25-years. For the projection, a system degradation factor of 0.54% in productivity each year was assumed, reducing the output to an absolute minimum of 86.5%. The hourly electricity grid emissions profile was not modified for future changes due to a lack of assumptions.

3 Results and Discussion

3.1 Electricity generation

Annual electricity generation ranges from 9.3-MWh to 18.2-MWh across the seven interconnection schemes, with final system efficiencies between 7.7% and 15.0%. The annual generation for each of the schemes is shown in Figure 6, where it is clear that MLC and DMC level optimisers lead to the most electricity generated. This is expected as the more optimisers present within a system, the better the potential loss from electrical mismatch can be mitigated. The worst performing scheme (SPF) involves the connection of group modules, organised by floor of the building, in series and then those series-strings in parallel. In contrast to the benefit of having a large quantity of optimisers in MLC and DMC schemes, SPF has the least. In between the best and least performing systems, there are two categories. The second-best-performing group are the schemes where the strings are first organised by column and then these are connected in parallel. The difference between the two schemes (SPC and TCT-C) in this group is minimal, but the non-cross-tied array yields slightly more. Then the schemes where the strings are arranged by row follow. These two, SPR and TCT-R, have a similar level near near-equal performance to the prior group with the non-cross-tied array performing slightly better.

These results indicate that the benefits of the cross-tie, which are generally seen in the literature, are not as prevalent in this array. This may be due to the cross ties being between strings instead of individual modules, which is more common. However, given the complexity of this facade, due to many different module sizes, it was necessary to avoid this type of tie in the study. A possible second explanation for this is that the benefits of the cross tie can often be seen using a higher-frequency MPPT. In this study, we simply extract the highest power per hour, but the reality is that MPPT algorithms must operate

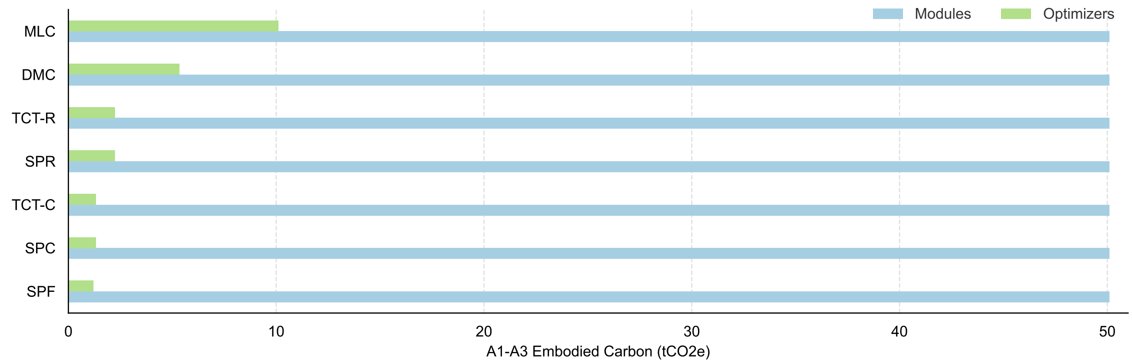

Figure 7: A comparison of the embodied carbon of the 31.235-kWp (164.8-m^2) PV array to the embodied carbon in each of the interconnections.

very quickly and consistently with respect to the placement of the MPP on the IV-curve.

3.2 Seasonality
The discussion of seasonality is particularly important in the Swiss context, where performance targets are being set for winter-time specific yield in PV plants. These targets and their incentives belong to Alpine-based deployment. However, the context of the discussion is equally important, as recommendations in Switzerland for building heating are based on the electrification. Additionally, there is an expectation that electricity demand will grow in the summer months due to increased cooling demand.

In Figure 6, we show the seasonal specific yield values for each of the schemes. Seasons were defined following a northern hemisphere convention: Winter-December, January, February; Spring-March, April, May; Summer-June, July, August; Autumn-September, October, November. The pattern that was observed in the results of the annual generation analysis are clear in this analysis as well. Schemes with more optimisers perform better no matter the season, those with fewer perform worse. The schemes with strings arranged in columns perform slightly better than those in row, and again the cross ties do not appear to have a substantial impact. We can also see, from the slope of the lines between the schemes, that the relative difference between the less well-performing schemes and the MLC and DMC is more substantial in the Summer and Spring seasons. This higher relative difference can also be seen in comparing the other schemes to each other. This can be attributed to the lower performing schemes not being able to mitigate the impact of heterogeneous irradiance conditions as well as MLC and DMC. This is exacerbated during the Spring and Summer months when direct irradiance is typically higher than the Fall and Winter. While the MLC and DMC schemes still perform better in the Winter, the relative difference between these two and the other schemes, which have less embodied carbon associated with their systems, is lower. This suggests that if designing for wintertime yields alone, it may be more important to focus on improving overall effective irradiance through system design features such as tilt.

3.3 Carbon abatement
As explained in Section 2.5 the electricity generated in each hour is used to mitigate the consumption of grid-based electricity, leading to the abatement of carbon emissions. The results are comparable to those in the annual generation analysis of Section 3.1. Due to the lack of seasonal differences in scheme performance, the relative abatement performance remains consistent across systems, from the worst to the best performing. We look at abatement using a single year's worth of generation data and the lifetime projected generation, but do not project changes to the grid emissions intensity. This is a limitation, but due to a lack of projection data for the regional electricity grid over the lifetime of the system, we permit this limitation with the acknowledgment that if projection data were used for the grid emissions then the comparative results between the schemes would remain the same. However, the absolute values of the abatement would likely be more realistic to expectations of the power market's development.

3.4 carbon payback time
As we can see from Figure 4 the smaller the capacity of the optimiser, the larger its embodied carbon per capacity rating, the full results of which can be seen in Figure 7. This results in the MLC and DMC

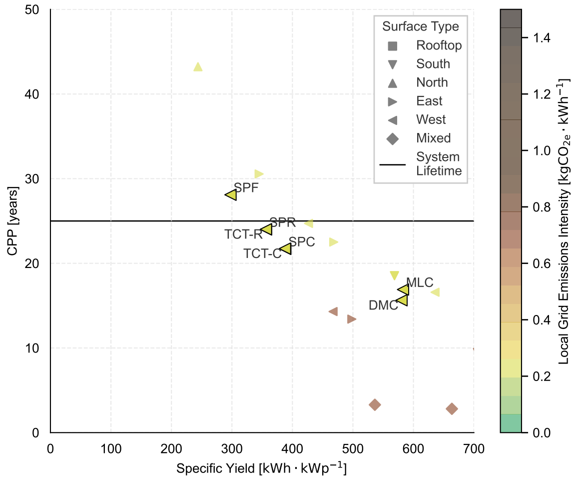

Figure 8: The calculated carbon payback time for each of the interconnections is compared to a subset of the data collected in the literature. The mixed category is of results from whole building studies where both monocrystalline and polycrystalline modules were installed on facades and rooftops—the results were only reported as an aggregate.

schemes having higher embodied carbon requirements than the other systems. This led to the initial hypothesis that the MLC and DMC would perform worse than other schemes in CPT. However we can see in Figure 8 that this is not the case. In opposition to the initial hypothesis, the schemes with more optimisers (MLC and DMC) perform the best. The additional electricity that is generated is substantial enough to offset their much larger "carbon debt". Generally though the results of this portion of the analysis follow the annual generation. With the other schemes, we see one case in which the CPT is longer than the lifetime of the system (SPF) and two in which is is within a year of the system's lifetime (TCT-R and SPR). Additionally, in Figure 8 we revisit the data collected in the literature review and shown in Figure 2 and compare a subset to the results of the interconnection analysis. We find that the resulting data is in a similar range to facades with similar orientations and in similar E_{int}.

4 Conclusion

In this study, seven BIPV interconnection schemes were evaluated through the comparative analysis of electricity generation and carbon abatement data using IV-curve-based simulations of a 31.235-kWp (164.8-m^2) monocrystalline PV array mounted on a SW-facing building facade in the urban context of Zurich, Switzerland. We considered the embodied carbon of the PV modules and the interconnection schemes, testing the hypothesis that systems with a higher number of power optimisers will have a slower time to offset their initial carbon cost than those with less power optimisers, despite their ability to reduce loss (i.e. generate more electricity) in urban settings. We find that systems with module-level power optimisers (MLC) and dual-module optimisers (DMC) have the largest embodied carbon values, but produce the most electricity. Despite the higher embodied carbon, their ability to mitigate loss due to electrical mismatch makes them the most effective options when viewed through a carbon emissions payback period (CPT) lens, refuting the initial hypothesis. Column-based interconnections perform slightly better than row-based ones, while the floor-based series-parallel scheme performs the worst. Cross-ties do not appear to substantially influence the results.

We evaluated the carbon abatement potential of each scheme using annual hourly grid emissions, representative of the EU and Switzerland, by assuming that each kWh generated, offsets a kWh from the grid. The findings indicate that while in some cases the CPT is less than the lifetime of the system, in other cases CPT is longer than the expected lifetime of the system. The best performing cases, MLC and DMC, optimise output for one or two modules given the conditions, whereas the other schemes must balance electrical mismatch within the individual strings of modules. For this we note that in some strings there may be better-performing modules whose performance is hindered by a lower-performing module. We posit that these string-based approaches may then be optimised further if lower-performing modules were never to be to installed within the array, but this was outside of the scope of the paper.

While our findings support the use of MLC and DMC optimisers for overall carbon mitigation efforts over the lifetime of the system, these approaches still require carbon emissions now, during a critical phase of the 1.5°C target. We did show that string-based approaches can be used to design a system that has a CPT of less than the lifetime of the system. For this reason we suggest that future research should pursue interconnection design for BIPV arrays that moves beyond the use of MLC's and towards optimal string layouts, which were not addressed in this study. Additionally, there is a lack of data surrounding inverter impacts, which we underscored in Section 2.5. A parametric calculator for assessing inverter and wire layout impact that is similar in implementation to Galimshina et al. (2024) [4] would further enable this type of analysis. Our analysis shows that an urban BIPV facade can be engineered in a way that worsens climate change, if the CPT exceeds the system's lifetime due upfront emissions being higher than those offset during operation. This is a challenge future research should address, possibly by shifting focus from efficiency gains to reducing energy and emissions intensive processes in manufacturing, even if it means accepting tradeoffs in efficiency.

Acknowledgments
This research was conducted at the Future Cities Lab Global at ETH Zurich. Future Cities Lab Global is supported and funded by the National Research Foundation, Prime Minister's Office, Singapore under its Campus for Research Excellence and Technological Enterprise (CREATE) programme and ETH Zurich (ETHZ), with additional contributions from the National University of Singapore (NUS), Nanyang Technological University (NTU), Singapore and the Singapore University of Technology and Design (SUTD).

References

1. McCarty J, Waibel C, and Schlueter A. Multi-Period Optimisation of District-Scale Building Integrated Photovoltaic Deployment. *IOP Conference Series: Earth and Environmental Science*. Sustainable Built Environment 2023. Vol. 1196. Journal of Physics: Conference Series. Publisher: IOP Publishing. Thessaloniki, Greece: IOP Publishing, 2023 Jun :012015. DOI: `10.1088/1755-1315/1196/1/012015`. Available from: `https://dx.doi.org/10.1088/1755-1315/1196/1/012015` [Accessed on: 2023 Jul 6]
2. Bau- und Liegenschaftsorgane der öffentlichen Bauherren (KBOB) K der. Ökobilanzdaten im Baubereich v6.2. Version 2009/1:2022, Version 6.2. 2024 Dec 3. Available from: `https://www.kbob.admin.ch/de/oekobilanzdaten-im-baubereich`
3. Leuchtturm: Photovoltaic Fassade an PlusEnergieBau Sanierung Zürich. Bern, Switzerland: Schweizer Bundesamt für Energie (BFE), 2019 Dec 18
4. Galimshina A, McCarty J, Waibel C, Schlueter A, and Hollberg A. High-resolution parametric embodied impact configurator for PV and BIPV systems. Renewable Energy. 2024 Dec 1; 236:121404. DOI: `10.1016/j.renene.2024.121404`. Available from: `https://www.sciencedirect.com/science/article/pii/S0960148124014721` [Accessed on: 2024 Sep 25]
5. Sinapis K, Tzikas C, Litjens G, Donker M van den, Folkerts W, Sark W van, and Smets A. A comprehensive study on partial shading response of c-Si modules and yield modeling of string inverter and module level power electronics. Solar Energy. 2016 Oct; 135:731–41. DOI: `10.1016/j.solener.2016.06.050`. Available from: `https://linkinghub.elsevier.com/retrieve/pii/S0038092X16302316` [Accessed on: 2022 Mar 14]
6. Ravyts S, Dalla Vecchia M, Van den Broeck G, and Driesen J. Review on Building-Integrated Photovoltaics Electrical System Requirements and Module-Integrated Converter Recommendations. Energies. 2019 Jan; 12. Number: 8 Publisher: Multidisciplinary Digital Publishing Institute:1532. DOI: `10.3390/en12081532`. Available from: `https://www.mdpi.com/1996-1073/12/8/1532` [Accessed on: 2022 Mar 14]
7. Sarkar D and Sadhu PK. Critical Comprehensive Performance Analysis of Static BIPV Array Configurations to Reduce Mismatch Loss and Enhance Maximum Power Under Partial Shading. IETE Technical Review. 2022 Oct 3; 0:1–33. DOI: `10.1080/02564602.2022.2127944`. Available from: `https://doi.org/10.1080/02564602.2022.2127944` [Accessed on: 2023 Jan 5]
8. Kumar S, Ahmad MS, Jalil MF, Tariq A, and Kirmani S. Comparative Analysis of Solar PV Array Under Mismatch Condition. *2023 International Conference on Power, Instrumentation, Energy and Control (PIECON)*. 2023 International Conference on Power, Instrumentation, Energy and Control (PIECON). 2023 Feb :1–6. DOI: `10.1109/PIECON56912.2023.10085803`. Available from: `https://ieeexplore.ieee.org/abstract/document/10085803?casa_token=Q5F11g15ccEAAAAA:mL-rN0NoniV98Nhy4lZfy8gAKvMQ4zI4kdVEToDYPfZdsZh_MxtECrWMQQF-GyY-U80D20IhCaK4` [Accessed on: 2025 Jan 13]

9. Freitas S, Serra F, and Brito MC. Pv layout optimization: String tiling using a multi-objective genetic algorithm. Solar Energy. 2015 Aug 1; 118:562–74. DOI: 10.1016/j.solener.2015.06.018. Available from: https://www.sciencedirect.com/science/article/pii/S0038092X15003266 [Accessed on: 2023 Jun 20]

10. Walker L, Hofer J, and Schlueter A. High-resolution, parametric BIPV and electrical systems modeling and design. Applied Energy. 2019 Mar; 238:164–79. DOI: 10.1016/j.apenergy.2018.12.088. Available from: https://linkinghub.elsevier.com/retrieve/pii/S0306261918319044 [Accessed on: 2022 Mar 14]

11. Waibel C, Mavromatidis G, Bollinger A, Evins R, and Carmeliet J. Sensitivity analysis on optimal placement of façade based photovoltaics. *Proceedings of the 31st international conference on efficiency, cost, optimization, simulation and environmental impact of energy systems.* ECOS 2018. Guimarães, Portugal: Universidade do Minho., 2018 :12 pp. Available from: https://www.dora.lib4ri.ch/empa/islandora/object/empa%3A22695/ [Accessed on: 2022 Nov 8]

12. Lu L and Yang H. Environmental payback time analysis of a roof-mounted building-integrated photovoltaic (BIPV) system in Hong Kong. Applied Energy. 2010 Dec; 87:3625–31. DOI: 10.1016/j.apenergy.2010.06.011. Available from: https://linkinghub.elsevier.com/retrieve/pii/S0306261910002254 [Accessed on: 2025 Apr 23]

13. Ma J. Dynamic Parametric LCA of BIPV Design. PhD thesis. Zurich: ETH Zurich, 2019

14. Amoruso FM and Schuetze T. Carbon Life Cycle Assessment and Costing of Building Integrated Photovoltaic Systems for Deep Low-Carbon Renovation. Sustainability. 2023 Jan; 15. Number: 12 Publisher: Multidisciplinary Digital Publishing Institute:9460. DOI: 10.3390/su15129460. Available from: https://www.mdpi.com/2071-1050/15/12/9460 [Accessed on: 2025 Apr 23]

15. Zurich S. 3D-Dachmodell LOD2. Zürich, 2018 Dec. Available from: https://www.stadt-zuerich.ch/geodaten/download/3D_Dachmodell_LoD2 [Accessed on: 2022 Apr 11]

16. Zürich GS. Baumkataster - Stadt Zürich. Zurich, 2022. Available from: https://www.stadt-zuerich.ch/ted/de/index/gsz/planung-und-bau/inventare-und-grundlagen/baumkataster.html [Accessed on: 2022 Jul 28]

17. Larson GW and Shakespeare R. Rendering with radiance: the art and science of lighting visualization. San Francisco, CA, USA: Morgan Kaufmann Publishers Inc., 1998

18. Subramaniam S. Daylighting Simulations with Radiance using Matrix-based Methods. Berkeley: LBNL Energy Technologies Area, 2017 Oct

19. Building CO. Zurich Airport TMYx. 2024. Available from: https://climate.onebuilding.org/WMO_Region_6_Europe/CHE_Switzerland/ZH_Zurich/CHE_ZH_Zurich.AP.066700_TMYx.zip

20. McCarty J, Waibel C, Leow SW, and Schlueter A. Towards a high resolution simulation framework for building integrated photovoltaics under partial shading in urban environments. Renewable Energy. 2024 Dec; 236:121442. DOI: 10.1016/j.renene.2024.121442. Available from: https://linkinghub.elsevier.com/retrieve/pii/S0960148124015106 [Accessed on: 2025 Jan 6]

21. Bishop J. Computer simulation of the effects of electrical mismatches in photovoltaic cell interconnection circuits. Solar Cells. 1988 Oct; 25:73–89. DOI: 10.1016/0379-6787(88)90059-2. Available from: https://linkinghub.elsevier.com/retrieve/pii/0379678788900592 [Accessed on: 2022 Jul 21]

22. Population Database - Eurostat. Available from: https://ec.europa.eu/eurostat/web/population-demography/demography-population-stock-balance/database [Accessed on: 2024 Sep 11]

23. Electricity Maps (2023). Electricity Maps Data Portal. 2025. Available from: https://portal.electricitymaps.com/datasets